# Sensor Ageing Impact on Finger-Vein Recognition

Christof Kauba, Andreas Uhl
Department of Computer Sciences, University of Salzburg
Jakob-Haringer-Str. 2, 5020 Salzburg, AUSTRIA
{ckauba, uhl}@cosy.sbg.ac.at

## Abstract

*The impact of sensor ageing related pixel defects on the performance of finger vein based recognition systems in terms of the EER (Equal Error Rate) is investigated. Therefore the defect growth rate per year for the sensor used to capture the data set was estimated. Based on this estimation an experimental study using several simulations with increasing numbers of stuck and hot pixels were done to determine the impact on different finger-vein matching schemes. Whereas for a reasonable number of pixel defects none of the methods is considerably influenced, the performance of several schemes drops if the number of defects is increased. The impact can be reduced using a simple denoising filter.*

## 1. Introduction

Biometric authentication systems become more and more widely used and important nowadays because of their advantages over password or token based ones. Besides the well established fingerprint recognition systems also authentication based on finger veins gains more attention. Finger-vein recognition utilizes the pattern of the blood vessels inside the fingers of a human which is captured using near infrared light. This has several advantages, e.g. resistance against forgery because the veins are underneath the skin and only visible in infrared light. Liveness detection is easily possible and the vein patterns are neither susceptible to abrasion nor finger surface conditions. Disadvantages include the rather big capturing devices compared to fingerprint sensors and images having low contrast and quality in general. Moreover, the vein structure can be influenced by temperature, physical activity and certain injuries and diseases.

Although finger surface conditions do not influence the results, the images can suffer from other distortions. One of these distortions are defective pixels due to ageing effects of the image sensor. These defects are point like, i.e. defects of single pixels where the most prominent types are hot pixels, followed by stuck pixels.

To the best of our knowledge, the impact of these pixel defects on the recognition performance of finger vein based recognition systems has not yet been studied. The contribution of this work is to investigate the impact of defective pixels due to sensor ageing on the recognition performance of different finger vein feature extraction and matching schemes in terms of the EER (Equal Error Rate). Actually this corresponds to investigating the robustness against point like, spiky shot noise.

At first, an estimation of the defect growth rate, based on the formula of Chapman et al. [4] using real sensor parameters of a finger vein scanner, was derived. Based on this we conducted several experiments using an ageing simulation algorithm. For the experiments the UTFVP [18] finger vein data set was used.

The rest of this paper is organised as follows: Section 2 describes image sensor ageing with its causes and presents the pixel defect model used for the simulations. Section 3 gives a brief overview of the finger vein feature extraction, matching and preprocessing methods. Section 4 describes the experimental settings, the simulation algorithm and provides the results with respect to the different schemes. Section 5 concludes this work.

## 2. Image Sensor Ageing

The main part of any digital imager is its image sensor. Most biometric sensors also contain some kind of image sensor, especially fingerprint, finger-, hand-vein scanners and iris scanners. There are two main types of image sensors, CCD and CMOS (APS). An image sensor is an analog device which basically consists of an array of photosensitive cells, called pixels. Like every human being and every electronic device also an image sensor ages. Image sensors develop more and more defective pixels as they become older even if they are not in use. These defective pixels show different characteristics than at manufacturing time. They appear as spiky noise in the output image. Pixel defects are permanent, their number increases linearly with time and they are randomly distributed over the sensor area.

## 2.1. Defect Causing Mechanism

According to the literature the main source causing the defects is assumed to be some constant external stress which impacts the image sensor. Albert Theuwissen [17] studied the influence of terrestrial cosmic rays on the number and the parameters of newly generated pixel defects in image sensors. He was able to show an increase in the hot spot density with increasing cosmic ray total flux. Leung et al. [11, 10] and Chapman et al. [2] applied statistical analysis to the spatial and temporal distribution of defects. They showed that the spatial distribution of defects across the sensor area follows a normal random distribution with no significant bias towards short or long distances, i.e. no defect clustering. They also showed that the number of defects increases linearly with time and inter-defect times follow an exponential distribution, indicating a constant defect rate which is both in contradiction to material degradation as defect source. Thus cosmic ray radiation, actually the neutrons of the cosmic rays, are the main source causing in-field sensor defects.

We focus on in-field defects only. There are also manufacture time defects which occur during the fabrication process. These defects may also include stuck and abnormal sensitivity pixels but are usually corrected by factory calibration, i.e. simply masked out.

## 2.2. Defect Types

The most prominent defect types that develop over a sensor's lifetime are hot and stuck pixels.

A **hot pixel** has an illumination independent component that increases linearly with exposure time. Whereas the dark response of a good pixel should be close to 0, the dark response of a hot pixel increases with exposure time. It appears as a bright spot with a fixed location in the output image. A partially-stuck hot pixel has an additional component (offset) that is independent from the illumination and exposure time. The main cause of a hot pixel is an increased dark current value compared to its neighbouring pixels due to the damage caused by cosmic ray radiation.

The output of a **stuck pixel** always has the same arbitrary but fixed value $c$ in the range $0 \leq c \leq 1$ (assumed pixel output range). Thus, a stuck pixel will always have the same output under all illuminations independent of the exposure time. Stuck pixels mainly appear as factory time defects.

## 2.3. Pixel Defect Model

A pixel model considers the incoming illumination and the impact of pixel defects on either the raw output of a single pixel or the whole sensor.

**Dudas, Leung and Chapman [5, 10, 3]** adopted the pixel model first proposed by Dudas et al. [5]. They claim that they have never found a true stuck pixel during their experiments. Thus their current pixel model only includes hot and partially-stuck hot pixels. Indeed they found out that partially-stuck hot pixels with a very high offset appear as stuck high. The output $I$ of a single pixel is:

$$I_{Pixel}(R_{photo}, R_{Dark}, T_{exp}, b) = m \cdot (R_{photo} \cdot T_{exp} + R_{Dark} \cdot T_{exp} + b) \quad (1)$$

where $R_{photo}$ measures the incident illumination, $R_{Dark}$ is the dark current rate, $T_{exp}$ is the exposure time, $b$ is the dark offset and $m$ is the amplification proportional to the ISO setting.

For an ideal good pixel, both $R_{Dark}$ and $b$ are 0 and the output is only proportional to the incident illumination. A standard hot pixel now adds a signal on top of the pixels output due to $R_{Dark} \neq 0$, whereas a partially-stuck hot pixel has an additional offset value $b \neq 0$. Therefore the output of the pixel will appear brighter.

Their former model also included stuck pixels and other defect types, where a stuck pixel was modelled (using an output range of a pixel between $0 - 1$ and $x = I_{photo} \cdot T_{integration}$; $I_{photo}$is the intensity of the incoming illumination and $T_{integration}$ the exposure time):

$$f_{Stuck-Mid}(x) = c, \;\; 0 < c < 1 \quad (2)$$

**Jessica Fridrich [6]** uses a more extensive pixel model:

$$Y = I + I \circ K + \tau D + C + \Theta \quad (3)$$
$$with \;\; Y, I, K, D, C, \Theta \in \mathbb{R}^{w \times h}; \tau \in \mathbb{R} \;\; and \; w, h \in \mathbb{Z}$$

where $Y$ is the sensor output, i.e. the image with dimensions $w \times h$, $I$ is the intensity of the incoming light (incident illumination), $I \circ K$ the photo-response non-uniformity PRNU, $\tau D$ the dark current (with $\tau$ being a multiplicative factor taking into account the exposure setting, sensor temperature, ...), $C$ is a light-independent offset and $\Theta$ is some additive modelling noise. According to this model, a pixel with an extremely high dark current value $D$ is called a hot pixel. Another defect type, the stuck pixel, has a high offset value $C$.

**Our Pixel Model** For this work we adopted the pixel model of Bergmüller et al. [1], which is a simplified version of Fridrich's pixel model and show that it is similar to the one of Dudas et al. Even if the models of Dudas et al. and Fridrich seem quite different at first sight, they are not. Dudas et al. simply do not include the PRNU and the additional modelling noise.

Since all pixels are independent and all operations are done element-wise, the matrix elements $y_{x,y} \in Y$ are denoted as $y \in Y$ for simplicity, the same for $i \in I$, $k \in K$,

$d \in D$, $c \in C$ and $\theta \in \Theta$. We are interested in the ageing effect of one specific sensor, thus the PRNU can be eliminated. As we aim for reproducible tests, modelling noise and environmental influences should be minimised, in fact they can be eliminated completely in a simulation, therefore $k = \theta = 0$. For all images taken with the sensor the same exposure settings are used, thus $\tau = const.$ and we set $\tau = 1$ for simplicity. The dark current level is low for short exposure times, usually used in standard photography but also for finger-vein images. Taking all this into account a simplified pixel model can be derived from Fridrich's pixel model:

$$y = i + d + c \;\; with \;\; y, i, c, d \in \mathbb{R} \tag{4}$$

If the dark current $d$ of a pixel is extremely high, it is often denoted as hot pixel. Whereas if the offset $c$ is high, this results in a saturated pixel and is sometimes denoted as stuck pixel (Dudas et al. denote this as partially-stuck hot pixel). As the definitions in the literature are not consistent, we define the following pixel model for our experiments:

$$y = c \tag{5}$$
$$y = i + d \tag{6}$$

where the first one is light independent and has a constant value $c$, denoted as stuck pixel. The second one adds an offset to the incident illumination and is referred as hot pixel. Hot pixels are caused by a higher dark current level compared to other pixels. The dark current level depends on the temperature and exposure time, which are both kept constant in our experiments, i.e. the dark current level is constant and thus there is no difference between a hot and a partially-stuck pixel, so it is simply denoted as hot pixel.

Our model for stuck pixels can be directly compared to the one used by Dudas et al. If you take their hot pixel model (see Equation 1), set $m = 1$, $T_{Exp} = 1$, $R_{Dark} = 0$ and set $I_{Pixel} = y$ , $R_{Photo} = i$ and $b = d$ (as discussed before) you get the same hot pixel model as we used.

This leads us to the following pixel model for 8 bit greyscale images:

$$Y(x,y) = \begin{cases} C(x,y) & if\, C(x,y) \neq 0 \\ I(x,y) + D(x,y) & otherwise \end{cases} \tag{7}$$
$$with \;\; Y, C, I, D \in (\mathbb{Z} : [0; 255]^{w \times h})$$

where $C$ and $D$ are the defect matrices. A pixel's output $Y(x, y)$ saturates at 0 and 255 if interval borders are exceeded. This pixel model is the basis for the ageing simulation algorithm, described in section 4.3.

### 2.4. Empiric Formula for Estimating Defect Growth Rate

Chapman et al. [4, 3] showed by continued empirical measurements of several imagers with different characteristics that the rate of pixel defects depends on the sensor technology (CCD or APS) and on sensor design parameters like sensor area, pixel size and gain (which is adjusted by the ISO setting). They derived the following formula:

$$D = A \cdot S^B \cdot ISO^C \tag{8}$$

where $D$ is the defect density (defects/year/mm²), $A$ is the number of defects/year/mm² if the pixel size is 1µm, $S$ is the pixel size, $ISO$ is the ISO value and $B$ and $C$ are constants depending on the sensor type. For a CCD sensor: $A = 0.0141$, $B = -2.25$ and $C = 0.69$ and for an APS sensor: $A = 0.0742$, $B = -3.07$ and $C = 0.5$.

## 3. Finger Vein Recognition

### 3.1. Preprocessing

Preprocessing can be grouped into methods to align the finger position and to improve the low contrast and image quality.

The first preprocessing method adopted from Lee et al. [9] (**LeeRegion**) simply masks out background pixels (setting them to 0). This is followed by a **normalization** step, i.e. rotation compensation as done in [7].

The second preprocessing stage tries to improve the image contrast. Simple **CLAHE** [21] or other local histogram equalization techniques are suggested by most authors for this purpose.

We use **High Frequency Emphasis Filtering (HFE)** which was originally proposed for hand vein image enhancement [20].

Filtering using a **Circular Gabor Filter** (**CGF**) as proposed by Zhang and Yang [19] was also applied as it leads to good results. For more details on the preprocessing and feature extraction methods the interested reader is referred to [8].

### 3.2. Feature Extraction and Matching

The first three techniques discussed here aim to extract the vein pattern from the background resulting in a binary image, followed by a comparison of these binary images using a correlation measure.

**Repeated Line Tracking** (RLT [14]) tries to track the veins as dark lines inside the image. Veins appear as valleys in the cross-sectional profile of the image. The tracking point is repeatedly initialised at random positions and then moved pixel by pixel along the dark line, where the depth of the valley indicates the movement direction. If no "valley" is detected a new tracking operation is started. The

number of times a pixel is tracked, is recorded in a matrix. Pixels that are tracked multiple times as belonging to a line statistically have a high likelihood of belonging to a blood vessel. Thus, binarisation using thresholding is applied to this matrix to get the binary output image.

**Maximum Curvature** (MC [15]) aims to emphasise only the centre lines of the veins and is therefore insensitive to varying vein width. The first step is the extraction of the centre positions of the veins. Therefore the local maximum curvature in the cross-sectional profiles, based on the first and second derivatives, are determined. Afterwards each profile is classified as being concave or convex where only local maxima in concave profiles indicate valid centre positions of the veins. Then a score according to the width and curvature of the vein region is assigned to each centre position, which is recorded in a matrix called locus space. Due to noise or other distortions some pixels may not have been classified correctly at the first step, thus the centre positions of the veins are connected using a filtering operation. Finally binarisation is done by thresholding using the median of the locus space.

**Wide Line Detector** (WLD [7]) is essentially an adaptive thresholding technique (using isotropic non-linear filtering), i.e. thresholding inside a local neighbourhood region. The difference of the centre pixel to its neighbours inside a circular neighbourhood and the number of pixels inside this neighbourhood with a difference smaller than a predefined threshold are determined. This number is again thresholded to get the final binary output vein image.

**Local Binary Patterns** (LBP [9]) is implemented as another representative of a binarisation-type feature extraction scheme. LBP compares the grey level of a centre pixel to its neighbouring pixels. Each pixel's grey scale value is then represented by the corresponding binary code resulting from the comparison with its neighbourhood.

To be able to qualify the impact on more basic schemes and the (eventual) advantages of the advanced ones, the last binarisation-type scheme tested is a simple **Adaptive Binarisation** (AB [16]) one.

For matching the binary feature images we adopted the approach in [14] and [15]. As the input images are not registered to each other and only coarsely aligned (rotation is compensated), the correlation between the input image and in x- and y-direction shifted versions of the reference image is calculated. The maximum of these correlation values is normalised and then used as final matching score.

In contrast to the techniques described above, key-point based techniques try to use information from the most discriminative points as well as considering the neighbourhood and context information of these points by extracting key-points and assigning a descriptor to each key-point. We used a **SIFT** [12] based technique with additional key-point filtering as in [8].

| Scheme | Preprocessing |
|---|---|
| SIFT | LeeRegion, Resize, CGF, HFE |
| MC, WLD, RLT, AB | LeeRegion, Normalization, Resize, CGF |
| LBP | LeeRegion, Norm, Resize, CGF, HFE, Denoising |

Table 1: Preprocessing for the Feature Extraction Schemes

## 4. Experiments

For MC, RLT and WLD we utilized the MATLAB implementation of B.T. Ton[1]. Table 1 shows the preprocessing methods applied for each of the evaluated feature extraction schemes.

### 4.1. Finger Vein Data Set

For the evaluation we used the University of Twente Finger Vascular Pattern Database (UTFVP) [18], kindly provided by R.N.J Veldhuis. It consists of a total of 1440 images, taken from 60 subjects, 6 fingers per subject and 4 images per finger. Their scanner uses a BCi5 monochrome CMOS camera[2] produced by C-Cam technologies. This camera has a CMOS image sensor with an active sensor area of $8.58 \times 6.86mm$, a pixel size of $6.7 \times 6.7\mu m$, a fill factor of $50\%$ and a resolution of $1280 \times 1024$ pixels.

### 4.2. Experimental Settings

Bergmüller et al. [1] had two iris data sets available, captured with a time span of four years in between. Therefore, they were able to estimate the relative growth in the number of defective pixels and their parameters from these data sets. They estimated a defect rate of $0.6659\,defects/MP/year$. Unfortunately, there are no two data sets with a time lapse in between for finger vein images taken with the same sensor. Thus, we used the formula of Chapman et al. [4] to estimate the defect growth rate based on the sensor data. There is no information available at which ISO level the UTFVP images were captured, therefore we assume ISO level $400$. Using this data yields a defect growth rate of:

$$D = 0.0742 \cdot 6.7^{-3.07} \cdot 400^{0.5} = 0.00432\,defects/year/mm^2 \quad (9)$$

or for a sensor area of $58.859mm^2$:

$$0.254\,defects/year = 0.194\,defects/MP/year \quad (10)$$

The finger-vein images have a resolution of $672 \times 380$ pixels. The effective pixel defect rate is:

[1]Publicly available on MATLAB Central: http://www.mathworks.nl/matlabcentral/fileexchange/authors/57311

[2]www.c-cam.be/doc/Archive/BCi5.pdf

$$\frac{672 \times 380}{1280 \times 1024} \cdot 0.254 = 0.0495\, defects/year \qquad (11)$$

According to Chapman et al. [3] and Albert Theuwissen [17] the additional offset $I_{Offset}$ of hot pixels or the dark current value, respectively follows an exponential distribution, i.e. hot pixels with a lower amplitude are more likely to occur. The parameter $\mu = 0.15$ of the exponential distribution was estimated using the data given in the papers of Theuwissen and Chapman et al.

Theoretically there would be only $0.0495\, defects/year$ caused by sensor ageing according to our defect model. But in practice much higher defect rates might occur due to other influences like higher ISO level, electrical stress or radiation originating from other sources. Moreoever, the cosmic ray total flux is dependent on the altitude, i.e. it increases with higher altitude. A realistic scenario with a high defect rate of more than $10\, defects/year$ would be a finger-vein based authentication system for air plane pilots because the flux is about 300 times higher on transatlantic flights than at ground level. At first we started the simulation with a defect rate of $1\, defect/year$. Such a low number of defects has little to no impact on the recognition accuracy. Therefore we then ran our simulations with a rate of $1000\, defects/year$, a time span of 10 years and a time step of 1 year to be able to quantify the impact of the pixel defects and to cover all scenarios where higher defect rates might occur, although such extremly high defect rates will hardly occur in practice.

### 4.3. Image Ageing Algorithm

We exclusively want to investigate the impact of sensor ageing related effects on the recognition performance and no additional effects like sensor conditions, subject or template ageing. Thus we used UTFVP images as a basis (unaged images) and simulated the sensor ageing related pixel defects. As our results are relative it does not matter if the UTFVP images already contain some defective pixels.

Although some researchers [5, 4, 3, 10] never found a true stuck pixel we included it in our simulations. We included hot and stuck pixels but no partially-stuck hot ones due to the assumed constant dark current level.

The following listing describes our sensor ageing algorithm in pseudo code, which is an extended version of the one proposed by Bermüller et al. [1] to generate the defect matrices $C$ and $D$ and also the sequence of aged images by applying these matrices to the input image $Y_{T_0}$ (can be applied to a set of source images to generate the aged data set) for a single source image and sample points in time $T_0 ... T_m$:

```
procedure AgedImageSequence(Y_T0)
  for i=1...m do
    Δn_s ← n_s(T_i − T_0) − n_s(T_{i−1} − T_0)
    Δn_ps ← n_ps(T_i − T_0) − n_ps(T_{i−1} − T_0)
    D_Ti = D_T{i−1}
    C_Ti = C_T{i−1}
    for k=1...Δn_s do
      r_a ← random in [0;1]
      do
        s_k ← random in w × h
      while checkNeighbours(s_k, 3) = 1
      C_Ti(s_k) ← r_a · a_s
    endfor
    for k=1...Δn_ps do
      r_a ← drawn from expd(0.15)
      do
        s_k ← random in w × h
      while checkNeighbours(s_k, 3) = 1
      D_Ti(s_k) ← r_a · a_ps
    endfor
    Y_Ti(x,y) = { C_Ti(x,y)              if C_Ti(x,y) ≠ 0;
                { Y_T0(x,y) + D_Ti(x,y)  otherwise.
  endfor
  return (Y_Ti)_{i=1...m}
end procedure
```

Our extensions include that the amplitude of the hot pixels is drawn from an exponential distribution, denoted as $expd(\mu)$ in the pseudo code and that $checkNeighbours(pos, size)$ is used to avoid local clustering of defects, i.e. no 2 defects are allowed to be inside the same $3 \times 3$ pixel region.

Actually, we would have to use the incident illumination $i$ according to our pixel model. As this is not known, we simply used the unaged images and injected the sensor ageing related hot and stuck pixels into the images, i.e. added a hot pixel offset $d$ to the pixel value and replace the pixel value by the value $c$ for stuck pixels.

### 4.4. EER Determination Procedure

The test procedure of the FVC2004 [13] was adopted to determine the EER.

For the genuine matches (FNMR) each image of each finger is compared with all remaining images of the same finger, no symmetric matches are performed. This results in a total of 2160 genuine matches.

For the impostor matches (FMR) the first image of each finger is compared against the corresponding first image of the same finger of all remaining subjects, again no symmetric matches are performed. This results in a total of 10620 impostor matches.

### 4.5. Experimental Results

We ran the simulations for hot pixels only, stuck pixels only and also combined stuck and hot pixels for MC, RLT,

| Method | EER | EER | 10000 Defects | 10000 Defects |
|---|---|---|---|---|
| | | w. denoising | | w. denoising |
| MC | 0.006 | 0.010 | 0.017 | 0.010 |
| RLT | 0.020 | 0.021 | 0.077 | 0.021 |
| WLD | 0.031 | 0.025 | 0.361 | 0.028 |
| LBP | 0.063 | 0.063 | 0.068 | 0.068 |
| SIFT | 0.020 | 0.022 | 0.029 | 0.023 |
| AB | 0.036 | 0.036 | 0.048 | 0.036 |

Table 2: EER Baseline and 10000 Defects

WLT, LBP, AB and the SIFT based approach. As the locations and amplitudes of the hot and stuck pixels are random we ran all tests 5 times and used the mean of the EER as final result. Furthermore, we did all the experiments with an additional denoising filter as preprocessing (median filter followed by an adaptive Wiener filter). LBP uses denoising during preprocessing by default thus the results for LBP are the same with and without denoising.

In Figure 1 some sample finger vein images containing no defects, 1000 and 10000 pixel defects and the corresponding region of the feature extraction image for MC, RLT and WLD are shown. One can clearly see that for MC due to the pixel defects the lines get broken and an additional line appears at 10000 defects which is clearly not a vein. The vein lines do not get broken for RLT but they appear wider with some additional noise at the vein boundaries. WLD does not show much useful information any more at 10000 defects due to the noise caused by the defective pixels which leads to dots and small circles inside the binary image.

Figure 2 shows that not only SIFT and MC but also the simple AB scheme (presumably because it relies on the finger outline and not only on the vein structure) is hardly influenced at all by hot pixel defects, even if there are 10000 defects inside the image. The EER of MC rises to 0.0074 at 10000 defects but it is still the best performing approach. The EER of RLT doubles at 10000 defects but stays still below 0.045. WLD, as it is quite a simple thresholding method, is influenced dramatically. At 10000 defects the EER is ten times higher than its baseline EER. The performance of LBP is hardly influenced at all by the noise introduced due to sensor ageing even in the case of 10000 defects.

In Figure 3 it can be seen that the influence of stuck pixels is higher than that of hot pixels. The average amplitude or hot pixel offset, respectively is quite low. Thus the original grey value is only slightly changed. Stuck pixels always have the same fixed value, independent of the original grey value, so they actually "break" the vein lines inside the image.

SIFT is again quite stable, while MC is affected more by stuck than by hot pixels and at 10000 defects the performance of MC gets worse than the SIFT one. Also the performance of AB is influenced more by stuck pixels than by hot ones as the EER rises to 0.051 at 10000 stuck defects in comparison to 0.043 for hot ones. RLT is even influenced more than MC and AB and its EER rises to 0.097 in comparison 0.045 at 10000 hot pixel defects. WLD is again highly influenced by the stuck pixel defects and like MC, AB and RLT even more than by hot pixel ones. The impact of stuck pixels on LBP is not higher than for hot pixel due to denoising.

If both, hot and stuck pixel defects, are present in the images, the results are similar to those for the single defect types. WLD is influenced most, whereas the performance of SIFT is quite stable, even if 20000 defects in total (10000

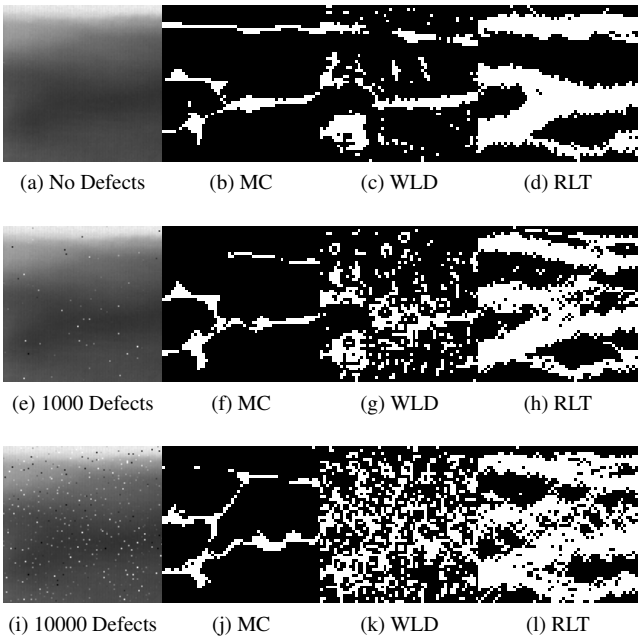


Figure 1: Sample Aged Images and Feature Extraction

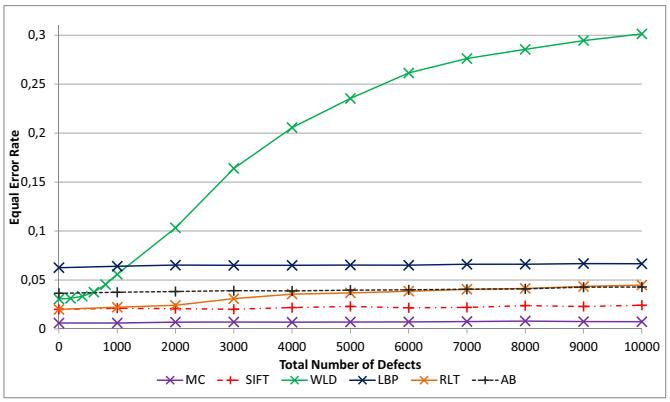


Figure 2: EER Hot Pixels only

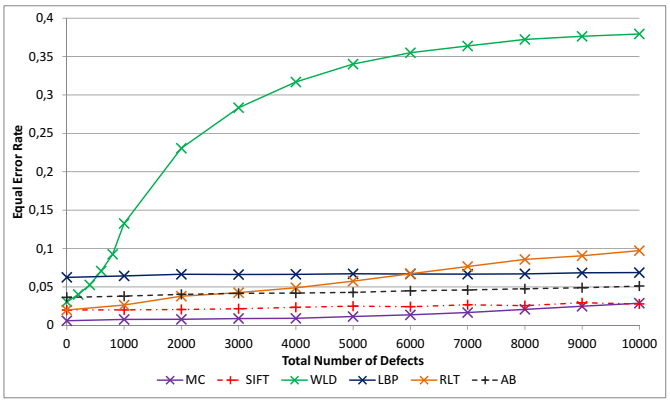


Figure 3: EER Stuck Pixels only

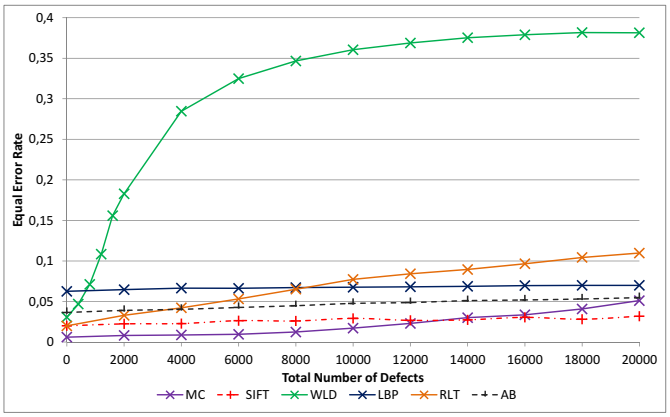


Figure 4: EER Hot and Stuck Pixels

hot and 10000 stuck pixels) are present, i.e. the EER only rises to 0.032. The performance of MC gets worse than SIFT for 14000 defects (MC: 0.03 and SIFT: 0.027). RLT is affected more than by hot pixels only but not as much as by stuck pixel defects only. Its EER for a total of 10000 defects is 0.077. The influence on LBP and AB is again negligible.

Table 2 shows that the baseline EER for MC, RLT and SIFT is slightly higher with denoising than without. It can be seen from Figures 5, 6 and 7, that the impact of sensor ageing related pixel defects can be eliminated almost completely using denoising for MC, SIFT, RLT and AB, i.e. the EER remains constant even for a high number of pixel defects, except some small statistical variations due to the random positions of the defective pixels. The EER of WLD and LBP rises only slightly. Denoising can be made adaptive such that it is only used at a certain noise level and in addition only used for schemes where it is advantageous. Thus the baseline EER stays the same and if more pixel defects are present, the EER can be reduced.

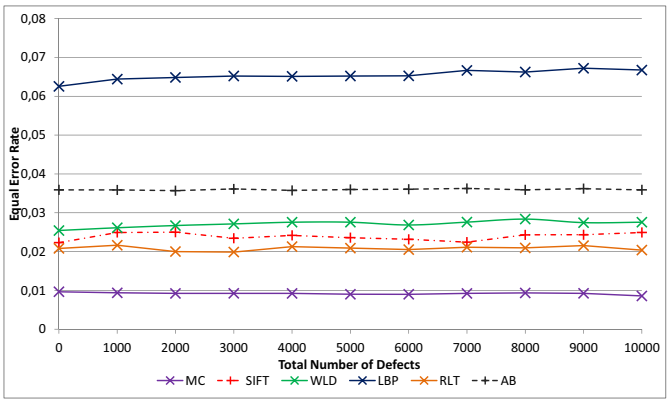


Figure 5: EER Hot Pixels only with Denoising

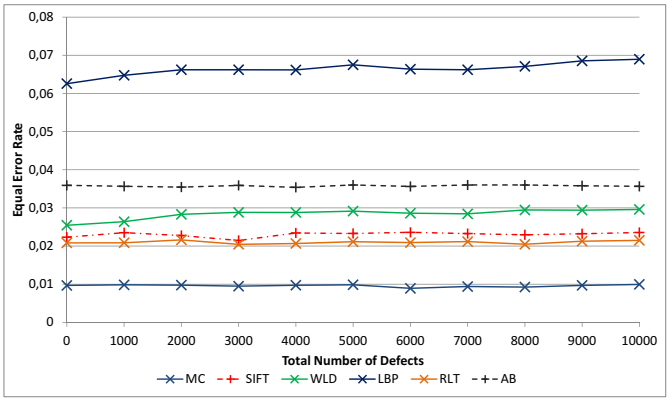


Figure 6: EER Stuck Pixels only with Denoising

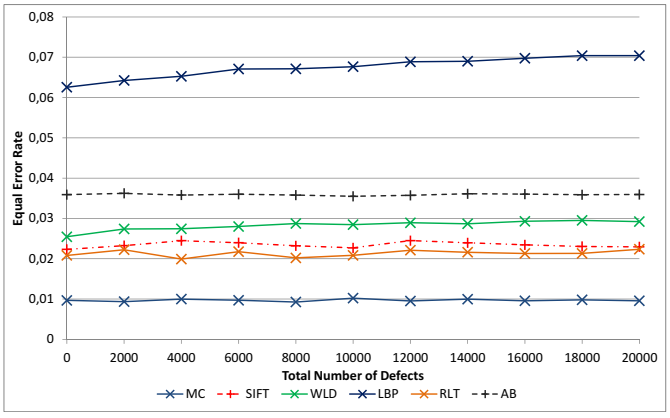


Figure 7: EER Hot and Stuck Pixels with Denoising

## 5. Conclusion

We used the UTFVP finger-vein dataset and several state of the art feature extraction and matching schemes to quantify the impact of sensor ageing related pixel defects on the performance of finger-vein based recognition systems. Our future work will include evaluations on other

publicly available datasets and further matching schemes. We showed that the impact of sensor ageing and its related pixel defects for a reasonable, i.e. realistic number of defective pixels which occurs in practice, is negligible. Thus sensor ageing is not an issue for practical applications of finger-vein recognition.

The theoretical defect rate of $0.05\,defects/year$ which hardly occurs in practice would lead to $1.5$ defective pixels over a reasonable long sensor lifetime of 30 years. In practice there are other factors such as higher altitudes, electrical stress and temperature changes leading to defect rates that are several hundred times higher. But the more advanced feature extraction and matching techniques are robust even against a high number of defects. At 10000 defective pixels SIFT is hardly influenced at all. Also MC, RLT, LBP and the simple AB scheme are quite robust against the defects. Only the performance of WLD drops significantly.

In addition a simple denoising filter is able to reduce the impact of pixel defects substantially at the cost of an increased baseline EER, i.e. a slight overall performance drop.

## Acknowledgements

This work has been partially supported by the Austrian Science Fund FWF, project no. P26630.

## References

[1] T. Bergmüller, L. Debiasi, A. Uhl, and Z. Sun. Impact of sensor ageing on iris recognition. In *Proceedings of the IAPR/IEEE International Joint Conference on Biometrics (IJCB'14)*, 2014.

[2] G. H. Chapman, I. Koren, and Z. Koren. Do more camera pixels result in a better picture? In *On-Line Testing Symposium (IOLTS), 2012 IEEE 18th International*, pages 73–78. IEEE, 2012.

[3] G. H. Chapman, J. Leung, A. Namburete, I. Koren, and Z. Koren. Predicting pixel defect rates based on image sensor parameters. In *Defect and Fault Tolerance in VLSI and Nanotechnology Systems (DFT), 2011 IEEE International Symposium on*, pages 408–416. IEEE, 2011.

[4] G. H. Chapman, R. Thomas, Z. Koren, and I. Koren. Empirical formula for rates of hot pixel defects based on pixel size, sensor area, and iso. In *IS&T/SPIE Electronic Imaging*, page 86590C. International Society for Optics and Photonics, 2013.

[5] J. Dudas, L. M. Wu, C. Jung, G. H. Chapman, Z. Koren, and I. Koren. Identification of in-field defect development in digital image sensors. In *Electronic Imaging 2007*, page 65020Y. International Society for Optics and Photonics, 2007.

[6] J. Fridrich. Sensor defects in digital image forensic. In *Digital Image Forensics*, pages 179–218. Springer, 2013.

[7] B. Huang, Y. Dai, R. Li, D. Tang, and W. Li. Finger-vein authentication based on wide line detector and pattern normalization. In *Pattern Recognition (ICPR), 2010 20th International Conference on*, pages 1269–1272. IEEE, 2010.

[8] C. Kauba, J. Reissig, and A. Uhl. Pre-processing cascades and fusion in finger vein recognition. In *Proceedings of the International Conference of the Biometrics Special Interest Group (BIOSIG'14)*, Darmstadt, Germany, Sept. 2014.

[9] E. C. Lee, H. C. Lee, and K. R. Park. Finger vein recognition using minutia-based alignment and local binary pattern-based feature extraction. *International Journal of Imaging Systems and Technology*, 19(3):179–186, 2009.

[10] J. Leung, G. H. Chapman, Z. Koren, and I. Koren. Statistical identification and analysis of defect development in digital imagers. In *IS&T/SPIE Electronic Imaging*, page 72500W. International Society for Optics and Photonics, 2009.

[11] J. Leung, J. Dudas, G. H. Chapman, I. Koren, and Z. Koren. Quantitative analysis of in-field defects in image sensor arrays. In *Defect and Fault-Tolerance in VLSI Systems, 2007. DFT'07. 22nd IEEE International Symposium on*, pages 526–534. IEEE, 2007.

[12] D. G. Lowe. Object recognition from local scale-invariant features. In *Computer vision, 1999. The proceedings of the seventh IEEE international conference on*, volume 2, pages 1150–1157. Ieee, 1999.

[13] D. Maio, D. Maltoni, R. Cappelli, J. L. Wayman, and A. K. Jain. Fvc2004: Third fingerprint verification competition. In *Biometric Authentication*, pages 1–7. Springer, 2004.

[14] N. Miura, A. Nagasaka, and T. Miyatake. Feature extraction of finger-vein patterns based on repeated line tracking and its application to personal identification. *Machine Vision and Applications*, 15(4):194–203, 2004.

[15] N. Miura, A. Nagasaka, and T. Miyatake. Extraction of finger-vein patterns using maximum curvature points in image profiles. *IEICE transactions on information and systems*, 90(8):1185–1194, 2007.

[16] N. Otsu. A threshold selection method from gray-level histograms. *Automatica*, 11(285-296):23–27, 1975.

[17] A. J. Theuwissen. Influence of terrestrial cosmic rays on the reliability of ccd image sensors-part 1: Experiments at room temperature. *Electron Devices, IEEE Transactions on*, 54(12):3260–3266, 2007.

[18] B. Ton and R. Veldhuis. A high quality finger vascular pattern dataset collected using a custom designed capturing device. In *International Conference on Biometrics, ICB 2013*. IEEE, 2013.

[19] J. Zhang and J. Yang. Finger-vein image enhancement based on combination of gray-level grouping and circular gabor filter. In *Information Engineering and Computer Science, 2009. ICIECS 2009. International Conference on*, pages 1–4. IEEE, 2009.

[20] J. Zhao, H. Tian, W. Xu, and X. Li. A new approach to hand vein image enhancement. In *Intelligent Computation Technology and Automation, 2009. ICICTA'09. Second International Conference on*, volume 1, pages 499–501. IEEE, 2009.

[21] K. Zuiderveld. Contrast limited adaptive histogram equalization. In *Graphics gems IV*, pages 474–485. Academic Press Professional, Inc., 1994.